LIP-STUDENTS-20-14

Sensitivity of LUX-ZEPLIN (LZ) to the neutrinoless double beta decay of ^{136}Xe

Helena Macedo[1,a], Inês Sequeira[1,b], and Tiago Martins[1,c]

[1] *Universidade de Coimbra, Coimbra, Portugal*

Project supervisor: P. Brás, A. Lindote

October 2020

Abstract. To this day, it is still unknown if neutrinos are Dirac or Majorana particles. The observation of the neutrinoless double beta decay process would potentially solve this problem and reveal Physics beyond the Standard Model. The LUX-ZEPLIN (LZ) experiment, whose main goal is the discovery of dark matter particle interactions, is capable of searching for other rare events as well, such as this decay. This study consists on the evaluation of the LZ sensitivity to the neutrinoless double beta decay of ^{136}Xe using a cut-and-count method and a simplified background model. Data sets from Monte Carlo simulations were analysed in order to optimize the detector performance and obtain the highest sensitivity possible in these conditions. A half-life sensitivity of 6.22×10^{25} years was obtained with this analysis for a simulated run lasting 1000 days.

Keywords: neutrinoless double beta decay, LZ, Majorana particles, neutrinos, mass hierarchy

1 Introduction

This study follows the work presented in the article "Projected sensitivity of the LUX-ZEPLIN experiment to the $0\nu\beta\beta$ decay of ^{136}Xe" [1].

1.1 Neutrinoless Double Beta Decay

Some isotopes, such as the ^{136}Xe, are known to undergo a process called double beta decay ($2\nu\beta\beta$), by which two neutrons from the nucleus are simultaneously transformed into two protons, emitting two electrons and two electron antineutrinos. However, there is another type of this decay that may be possible, but it still has not been observed: the neutrinoless double beta decay ($0\nu\beta\beta$). This process consists of the transformation of two neutrons into two protons with the emission of only two electrons. Figure 1 shows the Feynman diagram of the $0\nu\beta\beta$ decay. This decay mode is not allowed by the Standard Model and can only occur if neutrinos are Majorana particles, meaning that the neutrino is its own antiparticle [2, 3]. Since no neutrinos are emitted in this process, almost all of the energy of the decay will go into the two emitted electrons, with some small fraction going into the recoiling nucleus. Therefore, this process would result into a mono-energetic peak at the double beta decay Q-value ($Q_{\beta\beta} = 2457.83 \pm 0.37$ keV). The detection of the $0\nu\beta\beta$ decay would have major implications for Particle Physics and Cosmology, as it would be the first evidence of fundamental Majorana particles and would violate the conservation of lepton number and the B-L symmetry [2, 3]. This could possibly point to an explanation for the matter-antimatter asymmetry that is observed in the universe.

1.2 Mass Hierarchy

The Standard Model of particle physics predicts that neutrinos are massless particles. However, experimental observations of neutrino oscillations indicate that neutrinos do have mass. Neutrinos have three possible flavors and three mass states and they oscillate between them as they move through space, in a process called neutrino oscillation. These states are related to each other through a lepton mixing matrix (PMNS matrix):

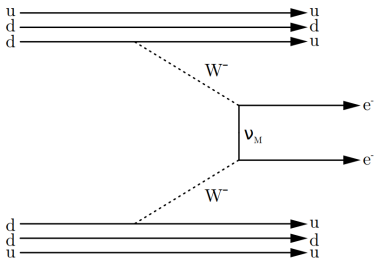

Figure 1. Feynman diagram of the $0\nu\beta\beta$ process due to the exchange of light massive Majorana neutrinos (ν_M). Figure from Reference [2].

$$\begin{bmatrix} \nu_e \\ \nu_\mu \\ \nu_\tau \end{bmatrix} = \begin{bmatrix} U_{e1} & U_{e2} & U_{e3} \\ U_{\mu 1} & U_{\mu 2} & U_{\mu 3} \\ U_{\tau 1} & U_{\tau 2} & U_{\tau 3} \end{bmatrix} \begin{bmatrix} \nu_1 \\ \nu_2 \\ \nu_3 \end{bmatrix}$$

and although their exact mass value is still unknown, this matrix provides access to some relations, displayed below.

$$m_1 < m_2 \tag{1}$$

$$|m_2 - m_1| << |m_3 - m_1| \tag{2}$$

As there is only information about the absolute value of the difference between two masses, there are two possible mass ordering options called hierarchies. The normal hierarchy states that $m_3 >> m_2 > m_1$, while the inverted hierarchy states that $m_3 << m_1 < m_2$ [2, 3]. The light neutrino exchange mechanism that might explain the neutrinoless double beta decay process is sensitive to the neutrino hierarchy via the effective Majorana mass ($m_{\beta\beta}$).

[a] e-mail: hlessamacedo@gmail.com
[b] e-mail: inesrsequeira@sapo.pt
[c] e-mail: tiago.m.martins@hotmail.com

2 The LZ Detector

The LUX-ZEPLIN (LZ) detector is already installed at the Sanford Underground Research Facility (SURF) and it is expected to start taking data in its first science run in 2021. The main science goal of LZ is the search for dark matter particle interactions, but its low-background environment makes it fitting for parallel searches of other rare events, such as the $0\nu\beta\beta$ decay of ^{136}Xe. For that search in particular, the detector must also have high abundance of the decaying element to compensate for the rareness of the event. A complete understanding of the existing backgrounds in the event search region is crucial, along with a good energy resolution at $Q_{\beta\beta}$. The active mass of LZ is equal to 7 tonnes of liquid xenon (LXe) that contains naturally occurring ^{136}Xe with an abundance of 8.9%, resulting in 623 kg of this isotope being naturally present in the TPC.

2.1 Operating Principle

The LZ experiment has a two-phase xenon time projection chamber (TPC). In this chamber, energy depositions produce prompt scintillation light (S1) and ionization electrons. The electrons that don't recombine with other xenon ions are drifted in an electric field and go towards the liquid surface. When they reach the liquid-gas interface, they are extracted by a stronger electric field into the gas phase where a second scintillation signal is created (S2). Both signals are detected by two arrays of photomultiplier tubes (PMTs), placed at the top and bottom of the active LXe target [4]. The time difference between both signals indicates the depth (z) of the interaction, while the relative intensity of the S2 pulse in each PMT of the top array is used to determine the position of the event in the horizontal (x, y) plane.

2.2 Structure

The TPC, schematically depicted in Figure 2, contains the active LXe mass and is the central section of LZ. The drift field is created by a voltage difference between a cathode grid located at the bottom of the chamber and a gate grid bellow the liquid surface. The electron extraction field, responsible for extracting the electrons into the gas region, is generated by the voltage difference between the gate grid and the anode grid placed above the liquid-gas interface [4]. Two arrays of PMTs placed at the extremities of the detector (253 in the top array and 241 in the bottom array) are responsible for observing the active region and collecting data. Furthermore, there is a bottom shield grid placed bellow the cathode, creating a reverse field region and protecting the bottom PMTs from high fields.

The TPC is surrounded by the xenon "skin" detector, an additional volume of xenon instrumented with PMTs, containing about 2 tonnes of LXe. Both the TPC and the skin detector are supported by a low-background double-walled titanium cryostat which is surrounded by the Outer Detector (OD), that contains 17 tonnes of organic liquid scintillator loaded with gadolinium [4]. The Gd has a high neutron capture cross-section and ensures that the OD has a high efficiency at vetoing neutrons. Finally, the entire LZ apparatus is immersed in a water tank that provides additional shielding to external neutrons and gamma-ray. The Skin and the OD are veto systems designed to detect radiation coming from the cavern walls and the detector components in order to exclude them from the analysis. A schematic of the full LZ detector is represented in Figure 3.

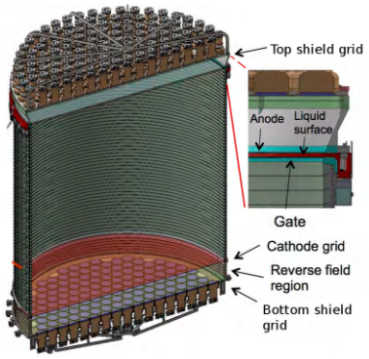

Figure 2. Schematic of the time projection chamber of LZ. Figure from Reference [5].

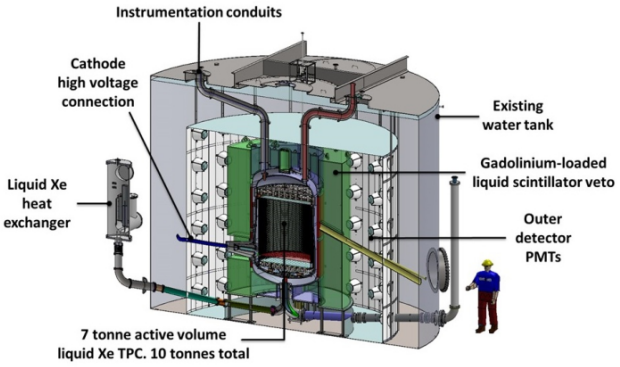

Figure 3. Schematic of the LZ detector. Figure from Reference [1].

3 Background Model

Extensive Monte Carlo simulations were generated in order to study the backgrounds in LZ from radioactive contamination in detector components, the cavern walls and those produced by cosmogenic processes. Once LZ starts collecting data, the backgrounds will be measured with high precision. The current background model takes into consideration contributions from the radiation from detector components, gamma rays from the cavern walls, neutron induced ^{137}Xe, internal ^{222}Rn, ^{136}Xe double beta decay and ^{8}B solar neutrinos [1, 6]. However, in the study presented here only the contributions of the radiation from detector components, which is expected to represent the main contribution to the total background rate, and the internal ^{222}Rn were taken into account. Figure 4 displays the full simulated background spectrum in the innermost

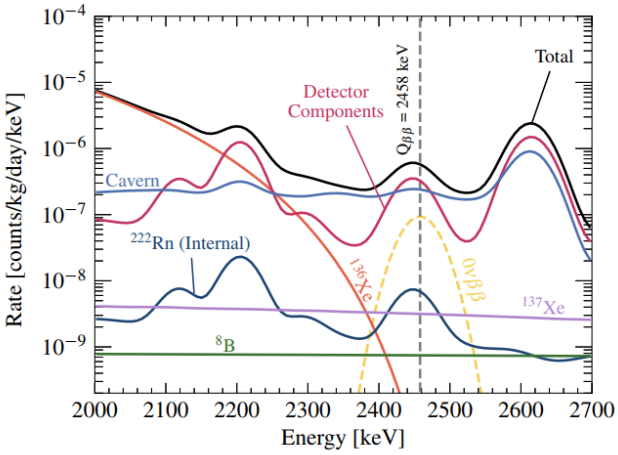

Figure 4. Energy spectrum of the main background sources. The dashed yellow line represents the expected signal for ^{136}Xe $0\nu\beta\beta$ decay, considering the expected sensitivity of LZ to the process. Figure from Reference [1].

region of the TPC (~1 tonne volume) in 1000 live-days of operation [1].

3.1 Detector Components

The background model includes contributions from most components of the TPC, skin, OD and other auxiliary systems of LZ. The detector was built with ultra-pure materials in order to reduce this type of background, but it still has big effect on the collected data. Amongst the detector components, the TPC PMTs are those with the largest contribution to the background [1].

Internal Radon

Residual dust and radioactive contamination from detector materials in the internal surfaces of the TPC emanate Radon from the decay chains of ^{238}U and ^{232}Th, that can diffuse into the TPC and mix with the LXe.

^{214}Bi is one of the daughters of the ^{222}Rn, and despite not being possible to separate its 2447 keV gamma line from the $0\nu\beta\beta$ region of interest (ROI) only by energy resolution, a coincident β decay can be used to veto this gamma line for well-centralized events in the TPC. ^{214}Bi also originates another problematic background, called "naked-β decay" (a β decay with no γ emission), that cannot be separated by energy resolution, as it will most likely produce a single-scatter event in the ROI [1]. This background can be excluded by removing events with either a dead time greater than 2.5 ms or the detection of an α, since the daughter ^{214}Po decays by α emission.

Another background derived from the internal radon comes from the decay of some positively charged ^{222}Rn daughters, that can drift to the cathode or deposit in the wall of the TPC, whose 2447 keV gamma line can originate a background that cannot be vetoed by a coincident beta or daughter decay [6].

4 Experimental Procedure

4.1 Methodology

The detector half-life sensitivity to the $0\nu\beta\beta$ signal is defined as the median 90% confidence level (CL) upper limit on the number of signal events that would be obtained from a repeated set of background-only experiments, assuming 1000 days of detector live time. For this analysis, a set of data obtained through Monte Carlo simulations of a full 1000 day run of LZ is used to estimate the sensitivity to the $0\nu\beta\beta$ decay of ^{136}Xe, considering only the contributions of radiation from detector components and the internal ^{222}Rn. A simplified cut-and-count analysis was used to estimate the sensitivity of LZ to this decay process [7]. This analysis also includes the optimization of the event selection cuts used to estimate the sensitivity. The optimization was performed iteratively for every available selection cut.

4.2 Selection Criteria

To estimate the impact of background events on the detector's exposition to signal, a multidimensional background model is used where each background is analysed based on energy ($2.1 < E < 2.9$ MeV), depth ($0 < z < 146$ cm), and radial position ($0 < r < 73$ cm). The following criteria are applied to the obtained simulations in order to reject as much background events as possible.

Fiducial Volume

The fiducial volume (FV) optimization consists in finding the compromise between xenon mass and background rejection that results on the highest detector sensitivity. Its effectiveness is related to the fact that external sources will produce higher backgrounds near the edges of the detector, since the xenon provides a self-shielding effect that results in lower background rates in the innermost regions.

Single-Scatter Cut

The expected $0\nu\beta\beta$ signal is point-like, resulting in mostly single-scatters. Therefore, it is reasonable to exclude multi-scatter interactions, which is done by rejecting events whose vertices are separated by a certain maximum vertical distance. This value corresponds to the single scatter cut and it is particularly useful to distinguish signal events from γ-ray interactions that will often scatter more than once in the TPC and produce multiple-scatter interactions. The default value used for this cut was 3 mm, and its effect in the sensitivity is further discussed in section 5.3.

Veto Systems

The veto systems consist of the detector Skin and Outer Detector [4]. $0\nu\beta\beta$ decays will not produce signal in these volumes, therefore, events that deposit energies higher than 100 keV on a time frame shorter than 1 μs on one of those systems are rejected [1].

Not all background events are removed by applying these criteria: the remaining ones are very "signal-like" and are expected to have a near uniform spatial distribution. Therefore, they can only be excluded by setting an energy window around $Q_{\beta\beta}$, which corresponds to the region of interest (ROI). The width of this energy window was chosen to be $\pm 1\sigma$ around $Q_{\beta\beta}$ and an assumed energy resolution of 1% (see further discussion in section 5.2).

5 Data Analysis

5.1 Fiducial Volume

The fiducial volume can be characterized based on three variables assuming that the detector has cylindrical symmetry: radius (r), and maximum and minimum height (z_{max} and z_{min}, respectively). Therefore, optimizing the fiducial volume means finding these three optimum values, which was done by applying an iterative process between r and the maximum and minimum z coordinates. Considering a set of values that represent approximately the whole detector as a starting point, the analysis was run for a sample of evenly separated r values while maintaining all other selection cuts at their nominal values, providing a list of the correspondent sensitivity values. After determining this roughly optimized r value, the analysis was run again for a sample of z_{max} and z_{min} values, now considering the r value previously obtained. Those values were used in order to improve the r optimization and so forth. This process was repeated until the values converged and the optimization was complete.

Although this analysis has the objective of eliminating as much background events as possible, the final volume cannot be too small. This is because it would contain a very small xenon mass and therefore limit the signal. Furthermore, it would mean that the sensitivity value would be associated to a very large uncertainty, and thus small variations on the cut values or fluctuations in the expected backgrounds would result on large variations on the sensitivity value.

Figure 5 represents the distribution of detected events inside and outside of the optimized fiducial volume. The total number of detected events within the final fiducial volume is only 8 events. The same observation is derived by observing the energy spectrum on Figure 6 by counting the number of events that survived all the cuts in the ROI. In addition to reducing the number of detected events, the FV optimization represented an improvement on the sensitivity value (Table 1), considering that the initial value was 8.35×10^{24} years for the first set of (r^2, z) values.

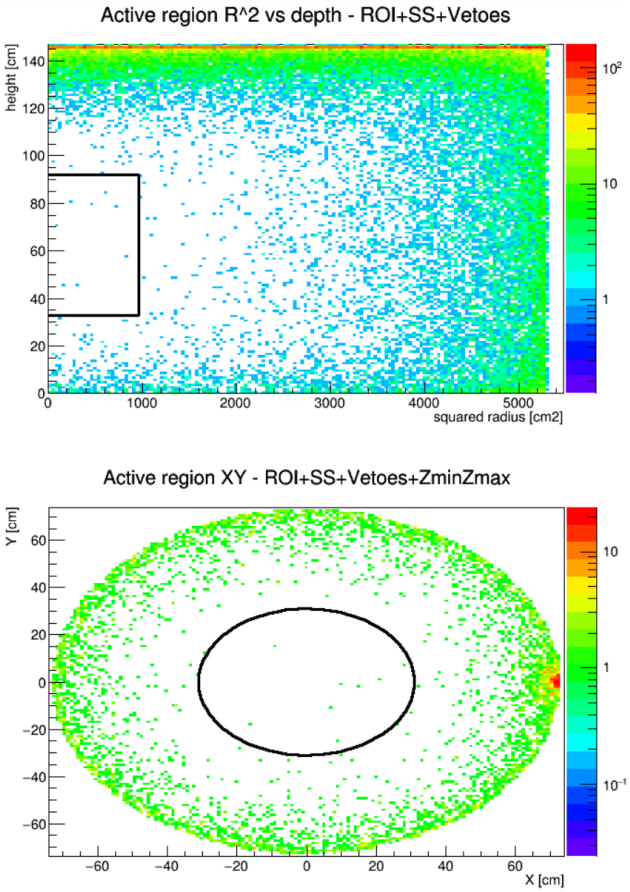

Figure 5. Background event counts on the active region and region of interest as a function of r^2 and z (top) and of x and y (bottom). The black line represents the optimized fiducial volume cut, outlining the region of the TPC where events are kept for further analysis.

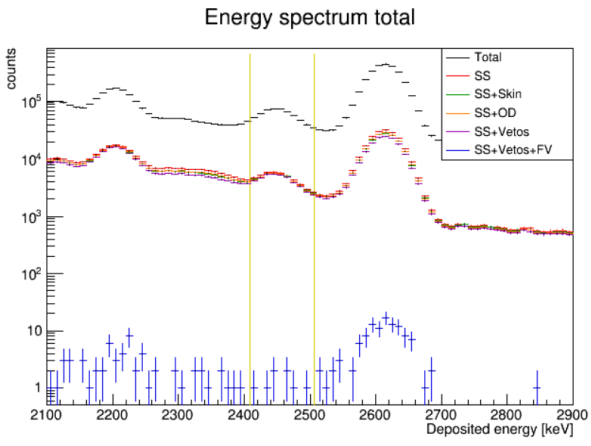

Figure 6. Background energy spectra. The vertical yellow lines represent the region of interest (ROI), which is the interval of energies equivalent to $\pm 1\sigma$ around $Q_{\beta\beta}$ for an energy resolution of 1%, expected to contain 68% of the $0\nu\beta\beta$ signal. The different spectra show the effect in background reduction from applying each of the cuts in succession.

5.2 Energy Resolution

To study the relation between the sensitivity and the energy resolution, a plot relating these two variables was made while keeping all other selection criteria constant and is shown in Figure 7. For this purpose, the fiducial volume found in the reference article was considered instead of the one found in this work, because although accounting for only a specific smaller region is essential for

Table 1. Detector dimensions and optimized values obtained in this analysis, taken from Reference [1] using the cut-and-count method and using the profile likelihood ratio (PLR) method [8], as well as the respective LXe mass (for a density of ~ 2.9 g cm^{-3}) and sensitivity.

	Detector	Optimized (this work)	Article (cut-and-count)	Article (PLR)
Height (cm)	147.0	59.0	70.0	130.6
Radius (cm)	73.5	31.0	39.0	68.8
LXe mass (kg)	7000.0	516.5	970.0	5632.1
^{136}Xe mass (kg)	623.0	46.0	86.3	501.3
Sensitivity (years)	–	6.22×10^{25}	7.40×10^{25}	1.06×10^{26}

eliminating backgrounds, the low number of events would increase the uncertainty of the plots. The obtained result shows (Figure 7) that the sensitivity decreases as the energy resolution worsens, confirming the predictions in [1]. This is to be expected, as a worse resolution leads to a wider ROI, and thus more background events are accepted.

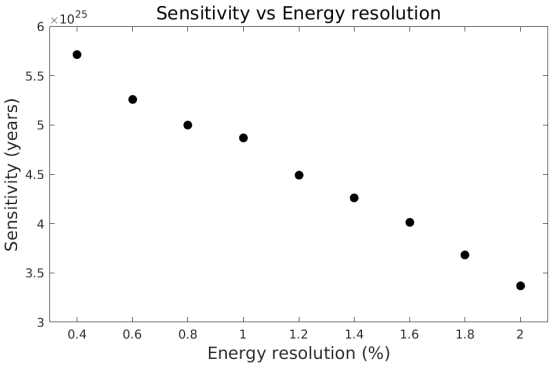

Figure 7. Variation of the sensitivity with the energy resolution at $Q_{\beta\beta}$. The projected resolution for the LZ experiment is 1% at $Q_{\beta\beta}$.

5.3 Minimum Vertical Vertex Separation

The relation between the sensitivity and the minimum vertical vertex separation was also explored. It was determined that for higher values of the vertical separation, more background events are allowed, worsening the sensitivity. On the other hand, having a very low value will result in the rejection of some signal events. Therefore, in both of these scenarios a decrease in sensitivity is observed. The trend obtained in the results, as shown in Figure 8, confirmed the expected behavior.

5.4 Improvement in the Energy Resolution and Minimum Vertical Separation

The assumed values for these parameters (1% energy resolution at $Q_{\beta\beta}$ and 3 mm of vertical separation) are not the ideal ones as can be seen from Figures 7 and 8 [1]. These values are derived from detector features and, because of that, these parameters are not easily improved without making drastic changes to the detector. Furthermore, the main goal of LZ is to study dark matter so the priority of the detector characteristics is not enhancing the

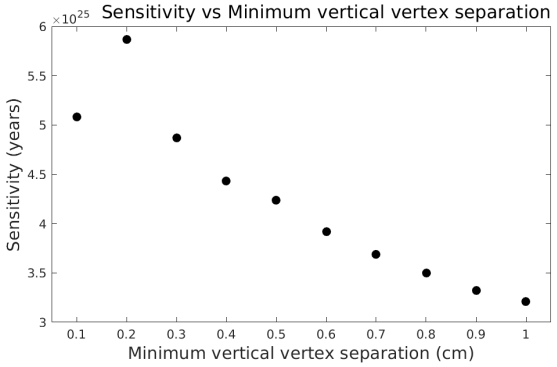

Figure 8. Variation of the sensitivity with the minimum vertical vertex separation. The assumed separation value for the LZ experiment is 3 mm.

sensitivity for this specific decay. Nevertheless, it is possible that both the energy resolution and the minimum vertex separation can be improved with more advanced algorithms applied to real data, resulting in a slightly higher sensitivity, since the assumptions made on this work are expected to be conservative. XENON1T, a detector similar to LZ, has demonstrated that an energy resolution of 0.8% is achievable at $Q_{\beta\beta}$ [9].

5.5 Veto Systems

To study the changes made by the veto systems (OD and Skin), the sensitivity obtained with different combinations of vetos was analysed. While the OD had a unnoticeable impact in the final result, a lower Skin threshold revealed an improvement on the sensitivity value. This is a consequence of taking into account only internal sources of background in the simulations, since the OD is especially efficient in removing exterior gamma rays, due to its peripheral location on the detector. In regard to the event count, the Skin contribution was equivalent to one extra event, which probably was originated from the detector materials, proving the importance of the Skin for eliminating background events from materials near the TPC.

5.6 Effective Majorana Mass

Knowing the value of the half-life sensitivity ($T^{0\nu}_{1/2}$), it is possible to use the relation [3]:

$$(T^{0\nu}_{1/2})^{-1} = \frac{\langle m_{\beta\beta}\rangle^2}{m_e^2} G^{0\nu} |M^{0\nu}|^2 \tag{3}$$

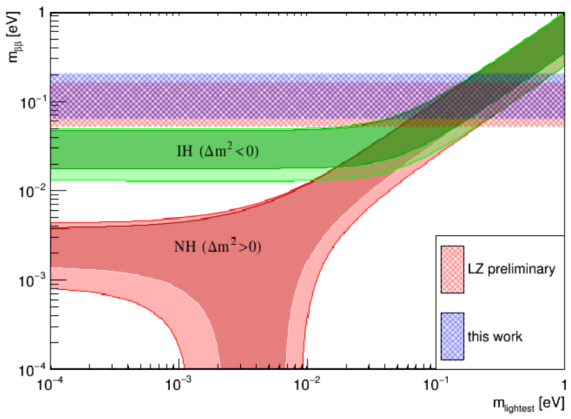

Figure 9. Projected LZ sensitivity to $m_{\beta\beta}$. IH and NH represent, respectively, the inverted and normal hierarchy neutrino mass scenarios. The two horizontal band represent the sensitivity of LZ obtained in the reference article (red) and in this work (blue).

to calculate an upper and lower limit to the Majorana effective mass. Using the optimized fiducial volume and the assumed values for the energy resolution and minimum vertical distance, an interval of 65 – 100 meV for the effective Majorana mass ($m_{\beta\beta}$) is obtained. The range of values of the effective mass is due to the uncertainty on the nuclear matrix elements ($M^{0\nu}$) [10, 11] . The graphic on Figure 9 can lead to important conclusions relative to the neutrino hierarchies. For instance, if the sensitivity to the $m_{\beta\beta}$ is smaller than the inverted hierarchy bandwidth and the decay is not observed, this hierarchy is excluded by this decay model.

6 Results and Conclusions

This analysis resulted in a fiducial volume equivalent to 516.5 kg of LXe, with the occurrence of eight events during 1000 days of live time and a half-life sensitivity of 6.22×10^{25} years to the $0\nu\beta\beta$ decay of ^{136}Xe. Furthermore, the obtained possible effective mass values have an interval of 65 – 200 meV. Regarding the values for the energy resolution and the minimum distance, while the curve shape is the same as the published results [1], the absolute values are different due to the different analysis methods used on each article.

In the reference article [1], the half-life sensitivity and the sensitivity to $m_{\beta\beta}$ of 53 – 164 meV were obtained with a more sophisticated statistical method. The difference in the results is a direct consequence of the method used in each analysis. The published result used a profile likelihood ratio method (PLR) [8] that employs probability density functions (PDF) that capture the nuances of the background distribution in both position and energy and results in a better signal-to-background discrimination than a simple cut-and-count analysis.

The current best experimental result obtained was in the KamLAND-ZEN experiment [12], with the half-life sensitivity of 1.07×10^{26} years. Comparing this result with the projected sensitivity for the LZ experiment it is noticeable the proximity between them. The sensitivity values and the bands for the effective Majorana mass show that the results obtained in this study, in spite of the simplified method used, were very close to the ones obtained on the reference article. Thus, this work shows that even with a simplified analysis, LZ can reach a competitive result for the search for this decay.

Acknowledgements

We would like to offer our special thanks to our project supervisors, Alexandre Lindote e Paulo Brás, for their availability and tireless work. We would also like to express our appreciation to all the internship program organisers, for making this experience possible and to LIP, for the amazing opportunity.

References

[1] D.S. Akerib et al. (LUX-ZEPLIN (LZ) Collaboration), Phys. Rev. C **102**, 014602 (2020), doi.org/10.1103/PhysRevC.102.014602

[2] S. Dell'Oro, S. Marcocci, M. Viel, F. Vissani, Advances in High Energy Physics (2016), doi:10.1155/2016/2162659

[3] M.J. Dolinski, A.W. Poon, W. Rodejohann, Annual Review of Nuclear and Particle Science **69**, 219 (2019), doi.org/10.1146/annurev-nucl-101918-023407

[4] D. Akerib et al. (LZ), Nucl. Instrum. Meth. A **953**, 163047 (2020), 1910.09124

[5] B.J. Mount et al., arXiv:1703.09144 (physics.ins-det) (2017), 1703.09144

[6] D. Akerib et al. (LZ), arXiv e-prints (2020), 2006.02506

[7] W.A. Rolke, A.M. Lopez, J. Conrad, Nucl. Instrum. Meth. A **551**, 493 (2005), physics/0403059

[8] G. Cowan, K. Cranmer, E. Gross, O. Vitells, Eur. Phys. J. **C71**, 1554 (2011), [Erratum: Eur. Phys. J.C73,2501(2013)], 1007.1727

[9] E. Aprile et al. (XENON), arXiv 2003.03825 (2020), 2003.03825

[10] N.L. Vaquero, T.R. Rodríguez, J.L. Egido, Phys. Rev. Lett. **111**, 142501 (2013)

[11] M.T. Mustonen, J. Engel, Phys. Rev. C **87**, 064302 (2013)

[12] A. Gando et al. (KamLAND-Zen Collaboration), Phys. Rev. Lett. **117**, 082503 (2016)